Elastic wave-vector decomposition using wave vector rotation in anisotropic media

Junxiao Li, Kristopher A. Innanen, Guo Tao and Laurence Lines

ABSTRACT

Elastic wave propagating in anisotropic media can be treated as a polarization deviation of wave vector in terms of isotropic media. The deviation angle between the wave normal and qP-wave's polarization direction can be estimated based on the phase angle and elastic constants(or Thomsen parameters). The anisotropic polarization vectors' components are thus determined according to the rotation matrix calculated by the deviation angle. The anisotropic wavefield-separation operators are constructed at each point using the calculated polarization vectors. Finally, the vector wavefield decomposition based on the Helmholtz theory are then used to decompose coupled qP- and SV- modes.

INTRODUCTION

True responses of elastic earth media are recorded by multicomponent seismic receivers. Elastic wave-equation migration for the recorded multicomponent data is able to provide more physically meaningful migration results, which are directly related to reflectivity and can thus be used to invert the physical parameters of reservoir rocks. The elastic reverse time migration (ERTM) can provide more accurate images than the acoustic RTM (Chang and McMechan, 1987; Chon et al., 2003; Lu et al., 2009). In general, P- and S-wave modes are mixed on all wavefield components and cause crosstalk and image artifacts. Yan and Sava (2008) suggest using cross-correlation imaging conditions of separated modes.

Research on P- and S-wavefield separation has been carried out for decades. The P-wavefield is curl-free and the S-wavefield is divergence-free in theory. Helmholtz decomposition (Morse et al., 1953) calculates potentials to determine decomposed vector modes, but this is applicable only for isotropic media and is not able to completely separate wave modes in anisotropic media. Dellinger and Etgen (1990) projected divergence and curl operators onto the mode polarization vectors in anisotropic media . However, the phases of the separated P- and S- components are both shifted by $\pi/2$ radian (Sun et al., 2001). Zhang and McMechan (2010) proposed a pragmatic decomposition of a vector wavefield based on the Helmholtz theory and the Christoffel equation which is used to calculate the polarization distribution, however, because the anisotropic phase polarization is local, the wavefield decomposition needs to be done separately for each region with different polarization distributions. (Rommel, 1994) proposed q-P- and q-SV-wave polarization vectors in 2D VTI media by solving Christoffel equation, but he pointed out that uncertainty exists when determining the polarization vector direction. Zhou (Zhou and Wang, 2016) proposed wave mode separation operators in anisotropic media, in which these operators are constructed by local rotation of wave vector polarization. The rotational angle is estimated using poynting vector (Dickens et al., 2011).

In this paper, we proposed a wavefield decomposed method based on the polarization

angle. For the polarization angle calculation in anisotropic media, the additional rotational angle is calculated according to Tsvankin(Tsvankin, 2012). The corresponding P- and S-components can thus be determined in terms of the polarization angle and the azimuthal angle. The 2D synthetic models in both isotropic and anisotropic media show the validity of the new scheme. The decomposed components are then used in ERTM to get imaging results for each reflection mode.

ELASTIC WAVE VECTOR DECOMPOSITION

Given any vector field $U(x, y, z)$, it can be decomposed into a curl-free part U^P and a divergence-free part U^S according to Helmholtz decomposition theory (Aki and Richards, 2002):

$$U = U^P + U^S, \tag{1}$$

with

$$\nabla \times U^P = 0, \tag{2}$$

and

$$\nabla \cdot U^S = 0, \tag{3}$$

in which, $\nabla = \frac{\partial}{\partial x}\boldsymbol{i} + \frac{\partial}{\partial y}\boldsymbol{j} + \frac{\partial}{\partial z}\boldsymbol{k}$. The divergence of the 3-D elastic wave field $\boldsymbol{U(x, y, z)}$ is

$$\nabla \cdot \boldsymbol{U} = \frac{\partial U_x}{\partial x} + \frac{\partial U_y}{\partial y} + \frac{\partial U_z}{\partial z}, \tag{4}$$

In the Fourier domain, the above equation is

$$\widehat{\nabla} \cdot \hat{\boldsymbol{U}} = ik_x\hat{U}_x + ik_y\hat{U}_y + ik_z\hat{U}_z, \tag{5}$$

where $\hat{\boldsymbol{U}}$ and $\widehat{\nabla}\cdot$ are the Fourier-domain forms of $\boldsymbol{U}$ and $\nabla\cdot$, respectively. $i = \sqrt{-1}$ and $\boldsymbol{k} = (k_x, k_y, k_z)$ are the wavenumber components at each direction. According to equation (2) and (3), for a P wave in Fourier domain, we have,

$$\widehat{\nabla} \cdot \hat{\boldsymbol{U}} = \widehat{\nabla} \cdot \hat{\boldsymbol{U}}^P. \tag{6}$$

Similarly, for an S wave in Fourier domain, we have,

$$\widehat{\nabla \times} \hat{\boldsymbol{U}} = \widehat{\nabla \times} \hat{\boldsymbol{U}}^S, \tag{7}$$

with $\hat{\boldsymbol{U}}^P = (\hat{U}_x^P, \hat{U}_y^P, \hat{U}_z^P)$ and $\hat{\boldsymbol{U}}^S = (\hat{U}_x^S, \hat{U}_y^S, \hat{U}_z^S)$ in the space domain as,

$$\boldsymbol{U}^P = U_x^P\boldsymbol{i} + U_y^P\boldsymbol{j} + U_z^P\boldsymbol{k}, \tag{8}$$

and

$$\boldsymbol{U}^S = U_x^S\boldsymbol{i} + U_y^S\boldsymbol{j} + U_z^S\boldsymbol{k}. \tag{9}$$

Based on the above equations, Zhang and McMechan (2010) proposed the solution for the three Fourier components of P-wavefield in isotropic media as

$$\begin{aligned}\hat{U_x^P} &= K_x^2\hat{U_x} + K_xK_y\hat{U_y} + K_xK_z\hat{U_z},\\ \hat{U_y^P} &= K_y^2\hat{U_y} + K_xK_y\hat{U_x} + K_yK_z\hat{U_z},\\ \hat{U_z^P} &= K_z^2\hat{U_z} + K_xK_z\hat{U_x} + K_yK_z\hat{U_y},\end{aligned} \tag{10}$$

with $\boldsymbol{K} = (K_x, K_y, K_z)$ being the normalized wavenumber components (e.g., $K_x = k_x/k, k = \sqrt{k_x^2 + k_y^2 + k_z^2}$). Similarly, the solution for the three Fourier components of S-wavefield in isotropic media are,

$$\begin{aligned}\hat{U_x^S} &= (K_y^2 + K_z^2)\hat{U_x} - K_xK_y\hat{U_y} - K_xK_z\hat{U_z},\\ \hat{U_y^S} &= (K_x^2 + K_z^2)\hat{U_y} - K_xK_y\hat{U_x} - K_yK_z\hat{U_z},\\ \hat{U_z^S} &= (K_x^2 + K_y^2)\hat{U_z} - K_xK_z\hat{U_z} - K_yK_z\hat{U_y},\end{aligned} \tag{11}$$

He also gives the vector forms of $\hat{\boldsymbol{U}^P}$ and $\hat{\boldsymbol{U}^S}$ as

$$\begin{aligned}\hat{\boldsymbol{U}^P} &= \boldsymbol{K}(\boldsymbol{K}\cdot\hat{\boldsymbol{U}}),\\ \hat{\boldsymbol{U}^S} &= -\boldsymbol{K}\times(\boldsymbol{K}\times\hat{\boldsymbol{U}}).\end{aligned} \tag{12}$$

In polar coordinate system, the wavenumber, polarization angle θ and azimuthal angle φ has the relationship as

$$(\sin\theta\cos\varphi, \sin\theta\sin\varphi, \cos\theta) = (K_x, K_y, K_z). \tag{13}$$

Therefor equation (6) and (10) can be expressed as

$$\begin{aligned}\hat{U_x^P} &= (\sin\theta\cos\varphi)^2\hat{U_x} + (\sin^2\theta\sin\varphi\cos\varphi)\hat{U_y} + (\sin\theta\cos\theta\cos\varphi)\hat{U_z},\\ \hat{U_y^P} &= (\sin\theta\sin\varphi)^2\hat{U_y} + (\sin^2\theta\sin\varphi\cos\varphi)\hat{U_x} + (\sin\theta\cos\theta\sin\varphi)\hat{U_z},\\ \hat{U_z^P} &= \cos^2\theta\hat{U_z} + (\sin\theta\cos\theta\cos\varphi)\hat{U_x} + (\sin\theta\cos\theta\sin\varphi)\hat{U_y},\end{aligned} \tag{14}$$

and

$$\hat{U_x^S} = (\sin^2\theta\sin^2\varphi + \cos^2\theta)\hat{U_x} - (\sin^2\theta\sin\varphi\cos\varphi)\hat{U_y} - (\sin\theta\cos\theta\cos\varphi)\hat{U_z},$$
$$\hat{U_y^S} = (\sin^2\theta\cos^2\varphi + \cos^2\theta)\hat{U_y} - (\sin^2\theta\sin\varphi\cos\varphi)\hat{U_x} - (\sin\theta\cos\theta\sin\varphi)\hat{U_z}, \quad (15)$$
$$\hat{U_z^S} = \sin^2\theta\hat{U_z} - (\sin\theta\cos\theta\cos\varphi)\hat{U_x} - (\sin\theta\cos\theta\sin\varphi)\hat{U_y},$$

In two dimensions (XOZ plane), based on the directional cosines $((\sin\theta, \cos\theta) = (K_x, , K_z))$, the decomposed P- and S-wavefield components are

$$\hat{U_x^P} = \sin^2\theta\hat{U_x} + \sin\theta\cos\theta\hat{U_z},$$
$$\hat{U_z^P} = \cos^2\theta\hat{U_z} + \sin\theta\cos\theta\hat{U_x}, \quad (16)$$

and

$$\hat{U_x^S} = \cos^2\theta\hat{U_x} - \sin\theta\cos\theta\hat{U_z},$$
$$\hat{U_z^S} = \sin^2\theta\hat{U_z} - \sin\theta\cos\theta\hat{U_y}, \quad (17)$$

Figure 1 (a) shows vertical and horizontal components (particle velocity) of one snapshot in a two-layer isotropic model using staggered-grid finite difference solution. The interface is set at 6 m depth. vp, vs and $density$ in each layer are shown in Table1

	$V_{P(m/s)}$	$V_{S(m/s)}$	$\rho_{(g/cm^3)}$
Upper layer	3450	1870	2.0
Lower layer	4000	2300	2.1

Figure 1 (b) and (c) show vertical and horizontal components of P- and S-mode acquired by equation (16) and (17), respectively. The amplitude and phase of the decomposed x- and z-components of the P- and S-waves are equal to those of input P- and S-wavefields. P- and S- mode have been precisely decomposed and they don't interference with each other.

In isotropic media, propagation direction and the polarization direction of P wave are completely parallel, but propagation direction and the polarization direction of S wave are completely perpendicular, so they are called "pure P wave" and "pure S wave". While in anisotropic media, there is usually a deviation of the polarization from the isotropic reference. This deviation can also be treated as an additional rotation $\Delta\theta$ of qP polarization angle $\theta + \Delta\theta$. In addition to particular direction, the propagation direction and polarization direction of P wave are not completely parallel but cut across each other; the propagation direction and the polarization direction of S wave are also not completely perpendicular, so called "qP wave" and "qS wave" (including SV wave and SH wave). Based on (Dellinger,

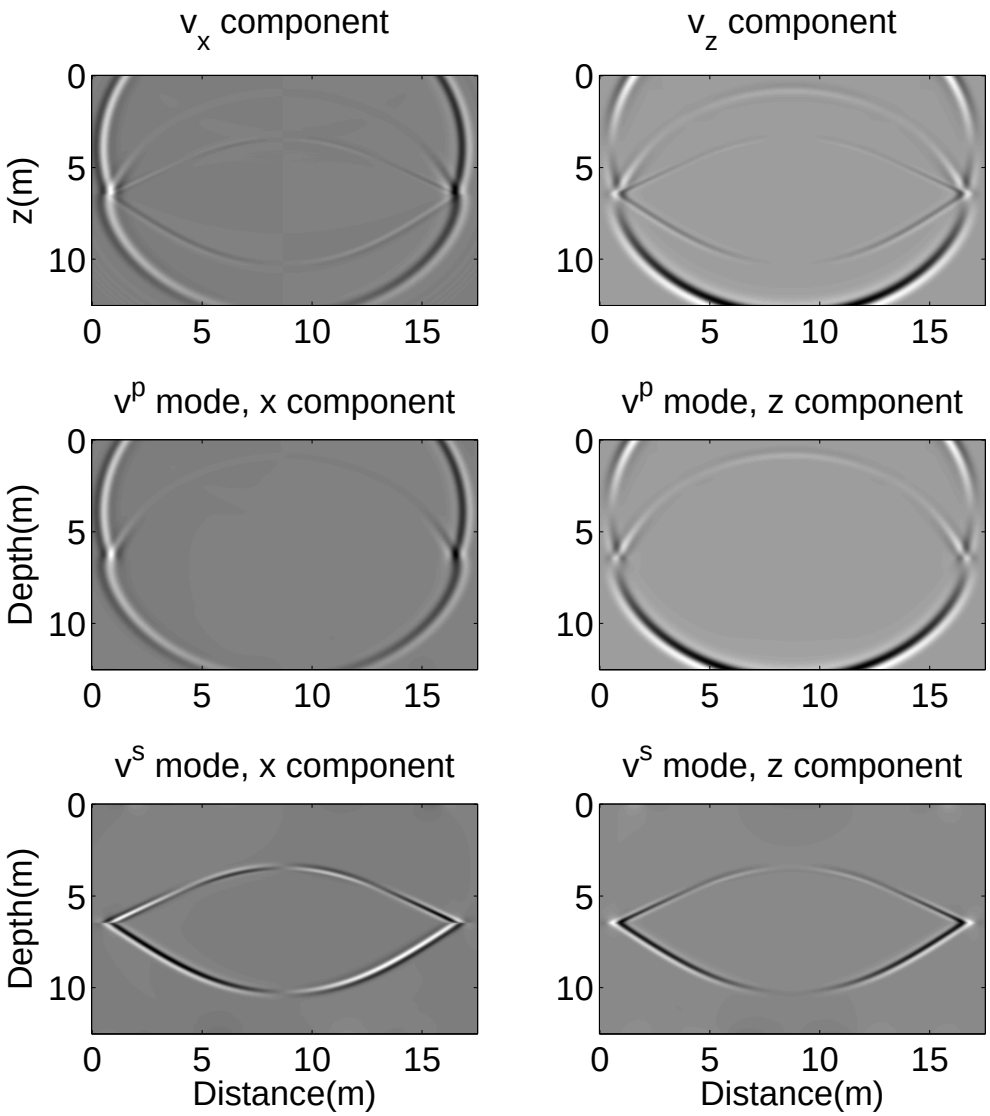

FIG. 1. 2D isotropic layered model (a) and

1991), Zhang and McMechan (2010) presented P- and S- wave vector decomposition forms as

$$\begin{aligned} \hat{\boldsymbol{U}^P} &= \boldsymbol{A^P}(\boldsymbol{A}^P \cdot \hat{\boldsymbol{U}}), \\ \hat{\boldsymbol{U}^S} &= -\boldsymbol{A^P} \times (\boldsymbol{A}^P \times \hat{\boldsymbol{U}}). \end{aligned} \tag{18}$$

where, $\boldsymbol{A^P} = (A_x^P, A_y^P, A_z^P)^T$ denotes the P-wave polarization vector. Assuming the polarization direction direction in anisotropic media is $\boldsymbol{A} = (A_x, A_y, A_z)^T$, the propagation direction is $\boldsymbol{n} = (\sin\theta\cos\varphi, \sin\theta\sin\varphi, \cos\theta)^T$, the angle between propagation direction and Z axis is θ and the azimuth angle of propagation direction is φ. Christoffel equation in anisotropic medium (Slawinski, 2003) is as follows

$$\begin{bmatrix} \Gamma_{11} - \rho V^2 & \Gamma_{12} & \Gamma_{13} \\ \Gamma_{12} & \Gamma_{22} - \rho V^2 & \Gamma_{23} \\ \Gamma_{13} & \Gamma_{23} & \Gamma_{33} - \rho V^2 \end{bmatrix} \begin{bmatrix} A_x \\ A_y \\ A_z \end{bmatrix} = 0 \tag{19}$$

with $\boldsymbol{\Gamma}$ in terms of the elasticity parameters C_{mn} as

$$\begin{aligned} \Gamma_{11} &= C_{11}n_1^2 + C_{66}n_2^2 + C_{55}n_3^2 + 2(C_{16}n_1n_2 + C_{56}n_2n_3 + C_{15}n_1n_3), \\ \Gamma_{22} &= C_{66}n_1^2 + C_{22}n_2^2 + C_{44}n_3^2 + 2(C_{26}n_1n_2 + C_{24}n_2n_3 + C_{46}n_1n_3), \\ \Gamma_{33} &= C_{55}n_1^2 + C_{44}n_2^2 + C_{33}n_3^2 + 2(C_{45}n_1n_2 + C_{34}n_2n_3 + C_{35}n_1n_3), \\ \Gamma_{12} &= \Gamma_{21} = C_{16}n_1^2 + C_{26}n_2^2 + C_{45}n_3^2 \\ &+(C_{12} + C_{66})n_1n_2 + (C_{25} + C_{46})n_2n_3 + (C_{14} + C_{56})n_1n_3, \\ \Gamma_{13} &= \Gamma_{31} = C_{15}n_1^2 + C_{46}n_2^2 + C_{35}n_3^2 \\ &+(C_{14} + C_{56})n_1n_2 + (C_{36} + C_{45})n_2n_3 + (C_{13} + C_{55})n_1n_3, \\ \Gamma_{23} &= \Gamma_{32} = C_{56}n_1^2 + C_{24}n_2^2 + C_{34}n_3^2 \\ &+(C_{25} + C_{46})n_1n_2 + (C_{23} + C_{44})n_2n_3 + (C_{36} + C_{45})n_1n_3, \end{aligned} \tag{20}$$

The P-wave polarization vector $\boldsymbol{A^P} = (A_x^P, A_y^P, A_z^P)^T$ is always polarized in symmetry axis planes which are formed by symmetry axis vector $\boldsymbol{n}$ and wave vector $\boldsymbol{k}$. As has discussed above, the P-wave polarization vector can be determined by rotating from wave vector $\boldsymbol{k}$ by an additional deviation angle $\Delta\theta$. According to the trigonometric relations, the rotated wave vectors $\boldsymbol{k'} = (k_x', k_z')$ can be expressed as

$$\boldsymbol{k'} = \boldsymbol{R}\boldsymbol{k}, \tag{21}$$

where, $\boldsymbol{R}$ is the rotation matrix with a rotation axis $\boldsymbol{u} = \frac{\boldsymbol{n}\times\boldsymbol{k}}{|\boldsymbol{n}\times\boldsymbol{k}|}$

For VTI media, the additional rotational angle $\Delta\theta$ can be represented by the expression (Tsvankin, 2012)

$$\Delta\theta = B\left[\delta + 2\left(\varepsilon - \delta\right)\sin^2\theta\right]\sin 2\theta. \tag{22}$$

where $B = \frac{1}{2\left(V_{S0}^2/V_{P0}^2\right)}$, ε and δ are Thomson parameters (Thomsen, 1986), V_{P0} and V_{P0} are the phase velocities which are perpendicular to isotropic plane of TI media. The above equation can also be expressed as

$$\Delta\theta = \frac{C_{33}}{C_{33} - C_{44}}\left[\delta\cos(2\theta) + 2\varepsilon\sin^2\theta\right]\sin\theta\cos\theta. \tag{23}$$

TTI media in observation coordinates can be derived from VTI(or HTI) media by the rotation of constitutive coordinates. In this paper, we assume the symmetry axis of TTI media lies in XOZ plane and $C_{11}^0, C_{33}^0, C_{13}^0, C_{44}^0, C_{66}^0$ are independent elastic parameters in VTI media in constitutive coordinates. For a TTI meidium with a nonzero tilt angle ν, the above equation can be expressed as

$$\Delta\theta = \frac{C_{33}}{C_{33} - C_{44}}\left[\delta\cos(2\theta - 2\nu) + 2\varepsilon\sin^2(\theta - \nu)\right]\sin\left(\theta - \nu\right)\cos\left(\theta - \nu\right). \tag{24}$$

Taking this deviation angle into equations (14) and (15), the qP- and qS- decomposed wave components can be expressed as

$$\begin{aligned}
\hat{U_x^{qP}} &= \left(\sin\left(\theta + \Delta\theta\right)\cos\varphi\right)^2\hat{U}_x + \left(\sin^2\left(\theta + \Delta\theta\right)\sin\varphi\cos\varphi\right)\hat{U}_y \\
&\quad + \left(\sin\left(\theta + \Delta\theta\right)\cos\left(\theta + \Delta\theta\right)\cos\varphi\right)\hat{U}_z, \\
\hat{U_y^{qP}} &= \left(\sin\left(\theta + \Delta\theta\right)\sin\varphi\right)^2\hat{U}_y + \left(\sin^2\left(\theta + \Delta\theta\right)\sin\varphi\cos\varphi\right)\hat{U}_x \\
&\quad + \left(\sin\left(\theta + \Delta\theta\right)\cos\left(\theta + \Delta\theta\right)\sin\varphi\right)\hat{U}_z, \\
\hat{U_z^{qP}} &= \cos^2\left(\theta + \Delta\theta\right)\hat{U}_z + \left(\sin\left(\theta + \Delta\theta\right)\cos\left(\theta + \Delta\theta\right)\cos\varphi\right)\hat{U}_x \\
&\quad + \left(\sin\left(\theta + \Delta\theta\right)\cos\left(\theta + \Delta\theta\right)\sin\varphi\right)\hat{U}_y,
\end{aligned} \tag{25}$$

and

$$\begin{aligned}
\hat{U_x^{qS}} &= (\sin^2(\theta+\Delta\theta)\sin^2\varphi + \cos^2(\theta+\Delta\theta))\hat{U_x} - (\sin^2(\theta+\Delta\theta)\sin\varphi\cos\varphi)\hat{U_y} \\
&\quad - (\sin(\theta+\Delta\theta)\cos(\theta+\Delta\theta)\cos\varphi)\hat{U_z}, \\
\hat{U_y^{qS}} &= (\sin^2(\theta+\Delta\theta)\cos^2\varphi + \cos^2(\theta+\Delta\theta))\hat{U_y} - (\sin^2(\theta+\Delta\theta)\sin\varphi\cos\varphi)\hat{U_x} \\
&\quad - (\sin(\theta+\Delta\theta)\cos(\theta+\Delta\theta)\sin\varphi)\hat{U_z}, \\
\hat{U_z^{qS}} &= \sin^2(\theta+\Delta\theta)\hat{U_z} - (\sin(\theta+\Delta\theta)\cos(\theta+\Delta\theta)\cos\varphi)\hat{U_x} \\
&\quad - (\sin(\theta+\Delta\theta)\cos(\theta+\Delta\theta)\sin\varphi)\hat{U_y}.
\end{aligned} \tag{26}$$

$\hat{\boldsymbol{U}^{qS}} = (\hat{U_x^{qS}}, \hat{U_y^{qS}}, \hat{U_z^{qS}})$ includes both SH- and qSV- waves. For the SH wave decomposition, setting the determinant of equation(19) as zero, the analytical phase velocity of qP-, qSV- and SH-waves in TTI media (Slawinski, 2003) are

$$\begin{aligned}
V_P &= \sqrt{\tfrac{1}{2\rho}\left[(C_{11}^0+C_{44}^0)F + (C_{33}^0+C_{44}^0)E^2 + \sqrt{D_{3D}}\right]}, \\
V_{SV} &= \sqrt{\tfrac{1}{2\rho}\left[(C_{11}^0+C_{44}^0)F + (C_{33}^0+C_{44}^0)E^2 - \sqrt{D_{3D}}\right]}, \\
V_{SH} &= \sqrt{\tfrac{1}{\rho}(C_{66}^0F + C_{44}^0E^2)},
\end{aligned} \tag{27}$$

where,

$$\begin{aligned}
D_{3D} &= [(C_{11}^0 - C_{44}^0)F - (C_{33}^0 - C_{44}^0)E^2]^2 + 4(C_{13}^0 + C_{44}^0)^2FE^2, \\
E &= (-sin(\theta+\Delta\theta)\cos\varphi\sin\nu + cos(\theta+\Delta\theta)\cos\nu), \\
F &= (sin(\theta+\Delta\theta)\cos\varphi\cos\nu + cos(\theta+\Delta\theta)\sin\nu)^2 + sin^2(\theta+\Delta\theta)\sin^2\varphi
\end{aligned} \tag{28}$$

Substituting SH wave phase velocity into Christoffel equations yields the general solutions of SH polarization (WU et al., 2010)

$$\boldsymbol{A}^{SH} = c\begin{bmatrix} \sin(\theta+\Delta\theta)\sin\varphi\cos\theta \\ -(\sin(\theta+\Delta\theta)\cos\varphi\cos\theta + \cos(\theta+\Delta\theta)\sin\theta) \\ \sin(\theta+\Delta\theta)\sin\varphi\sin\theta \end{bmatrix} \tag{29}$$

Therefore, the decomposed SH-wave can be determined by substituting the above matrix into the SH-wave polarization equation (Zhang and McMechan, 2010)

$$\hat{\boldsymbol{U}}^{SH} = \boldsymbol{A}^{SH}(\boldsymbol{A}^{SH}\cdot\hat{\boldsymbol{U}}), \tag{30}$$

$\boldsymbol{P}^{SH} \cdot \boldsymbol{n} = 0$ shows that the polarization direction of SH wave in VTI media is perpendicular to the propagation direction, which is called pure SH wave.

According to equations (25) and (26), the qP- and qSV- wave decomposition in XOZ plane can be determined as

$$\begin{aligned} \hat{U_x^{qP}} &= (\sin(\theta + \Delta\theta))^2 \hat{U_x} + (\sin(\theta + \Delta\theta)\cos(\theta + \Delta\theta))\hat{U_z}, \\ \hat{U_z^{qP}} &= \cos^2(\theta + \Delta\theta)\hat{U_z} + (\sin(\theta + \Delta\theta)\cos(\theta + \Delta\theta))\hat{U_x}, \end{aligned} \tag{31}$$

and

$$\begin{aligned} \hat{U_x^{qSV}} &= (\cos^2(\theta + \Delta\theta))\hat{U_x} - (\sin(\theta + \Delta\theta)\cos(\theta + \Delta\theta))\hat{U_z}, \\ \hat{U_z^{qSV}} &= \sin^2(\theta + \Delta\theta)\hat{U_z} - (\sin(\theta + \Delta\theta)\cos(\theta + \Delta\theta))\hat{U_x}. \end{aligned} \tag{32}$$

EXAMPLES

In this section, we illustrate the elastic wave-vector decomposition in anisotropic media with a synthetic model and elastic Sigsbee 2A model.

The 2D elastic graben model

Firstly, a simple graben model is used to test our wave-mode decomposition method. There are two horizontal layers and a graben structure, shown in Figure. The total grid number is 391×291 grids, including a PML layer of 20 grids at each boundary of this model. The model size is $17.55 \times 12.55\ m^2$, with a grid size of $0.05 \times 0.05\ m^2$. The time sample is $8\ \mu s$, and the total recording time is 14.4 ms. The source signal is represented by a Ricker wavelet with a dominant frequency of 3500 Hz. 26 shots are placed 1.5 m below the surface with an interval of 0.5 m, and 26 receivers are evenly distributed at the same depth with the source from 1.1 m to 13.6 m in x direction. The model and its parameters are shown in Figure 2 (a). Figure 2 (b) and (c) show the original polarization angle θ and its additional rotational angle $\Delta\theta$. The magnitude of angle Δ is normally smaller than 0.25 radians.

The normalized wavenumber K (Kx, Kz) are shown in Figure 3 (a) and (b). As is discussed, K denotes not only the wave-propagation direction but also the P-wave-polarization direction in isotropic media. In anisotropic media, the P- and SV- wave polarization vectors $\boldsymbol{A^P}$ and $\boldsymbol{A^{SV}}$ can be determined according to Rommel(Rommel, 1994), which are shown in Figure 3 (c)-(f). As Rommel pointed out in his paper, the direction of polarization vector $\boldsymbol{A_x^P}$ or $\boldsymbol{A_x^S V}$ is ambiguous, only absolute values of $\boldsymbol{A_x^P}$ or $\boldsymbol{A_x^S V}$ are shown. Compared with 3 (a) and (b), the directions of polarization vectors in isotropic layers (when kz <-0.5 and kz>0.8) have also changed. In contrast, the polarization vectors calculated by equation (16) and equation (17) are shown in Figure 4. Compared with Figure 3, the directions of polarization vectors in isotropic layers are the same as those in Figure 3 (a) and (b), and

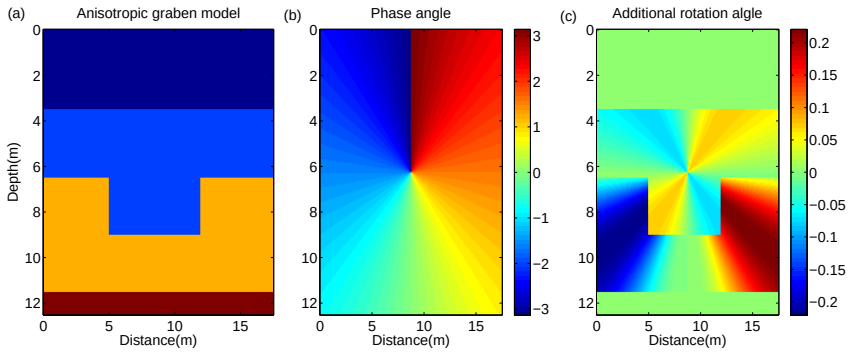

FIG. 2. (a) 2D anisotropic graben model, (b) the original polarization angle and (c) additional rotational angle.

they change slightly in anisotropic layers (roughly when -0.5<kz<0.8) because of an additional rotation. But the signs of these vectors keep unchanged as the rotational angle is relatively small, which differs from 3 (c)-(f). By implementing our new proposed method, the decomposed wavefield components can be obtained.

The upper two of Figure 5 show the vertical and horizontal components of elastic wavefield snapshots using staggered-grid finite difference solution. The P- and S- modes are mixed in both components. The middle two of Figure 5 show the x- and z-components of the decomposed P-wave, the P-mode that travels faster than the S mode, which performs as an envelope outside S-mode. The decomposed S- components in x- and z- direction are illustrated in the last two of Figure 5, where the shape of S-mode in different propagation distances submerges. The decomposed x- and z-components of P-and SV-waves don't include each other. The components are well separated with the phase, amplitude and physical units unchanged.

The 2D anisotropic thrust fault model

The second model is a thrust fault model, in which anisotropy present through different depth intervals. The upper right picture of Figure 6 shows the original velocity component $\boldsymbol{v_x}$, the model is shown as background layers, the P- and S- waves are mixed with each other especially in the sharp structural areas. The S mode can barley detected in the interior layers of the model, in contrast, the lower left picture of Figure 6 shows the decomposed S wave component $\boldsymbol{vs_x}$, which shows clear S mode propagation in both sharp areas interior layers. The combination between the decomposed $\boldsymbol{vp_x}$ and $\boldsymbol{vs_x}$ on the lower right of Figure 6 has the same phase and amplitude with the original $\boldsymbol{v_x}$ mode (upper right picture of Figure 6). Figure 7 shows the decomposed P- and S- wave components $\boldsymbol{vp_z}$ and $\boldsymbol{vs_z}$ as well as the original $\boldsymbol{v_z}$ before decomposition.

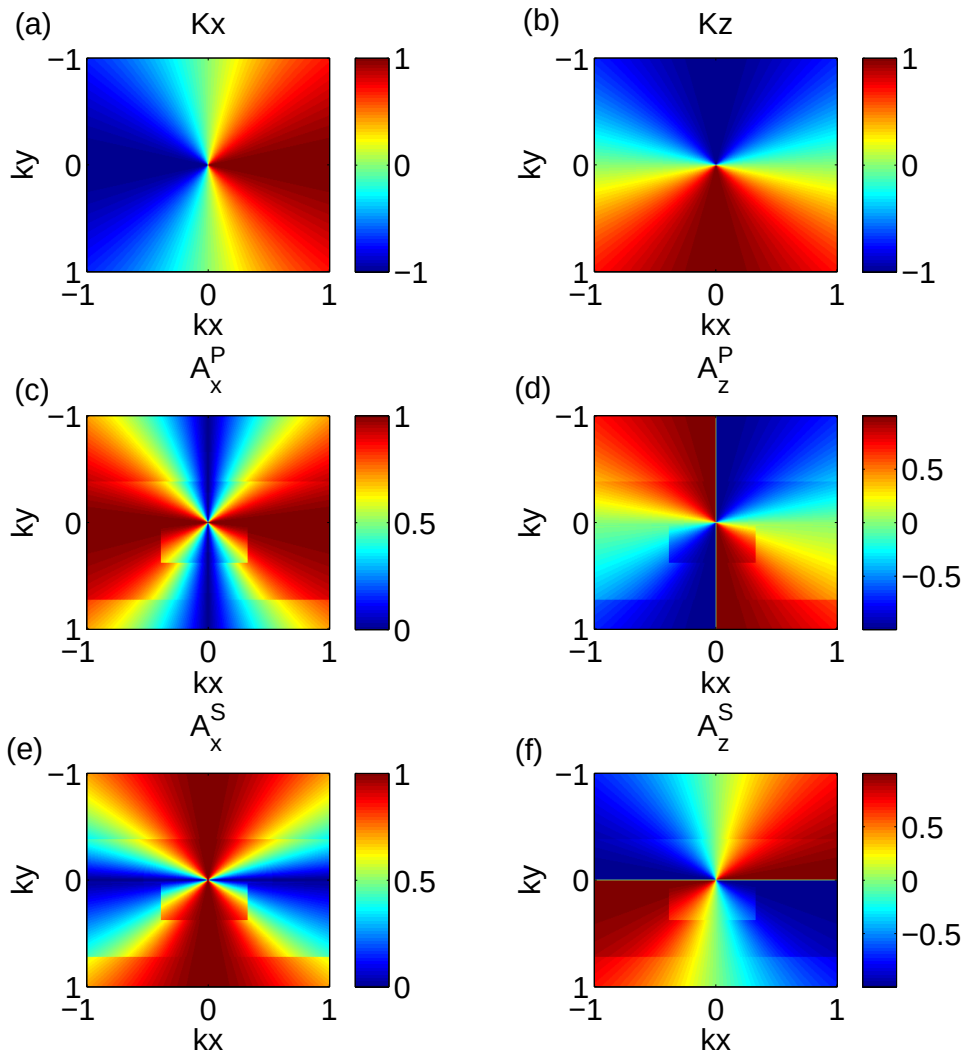

FIG. 3. (a)-(b) The normalized wavenumber K and (c)-(f) the P- and SV- wave polarization vectors in VTI media according to Rommel. Compared with (a) and (b), the directions of polarization vectors in isotropic layers (when kz <-0.5 and kz>0.8) have also changed.

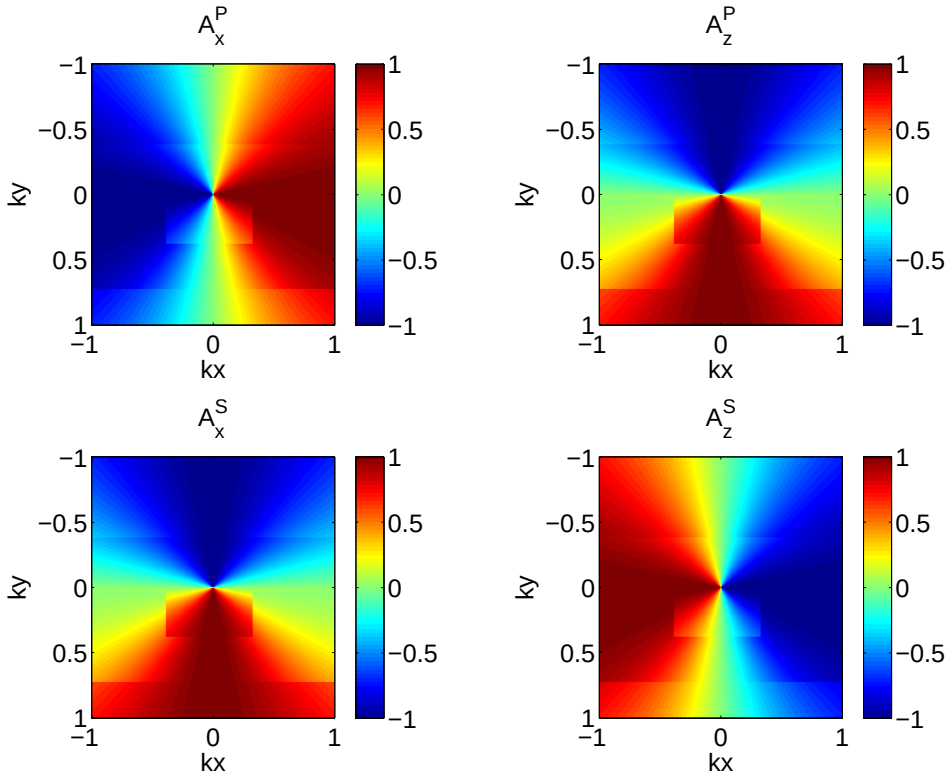

FIG. 4. The P- and SV- wave polarization vectors in VTI media according to equation (16) and equation (17), the directions of polarization vectors in isotropic layers are the same as those in Figure 3 (a) and (b).

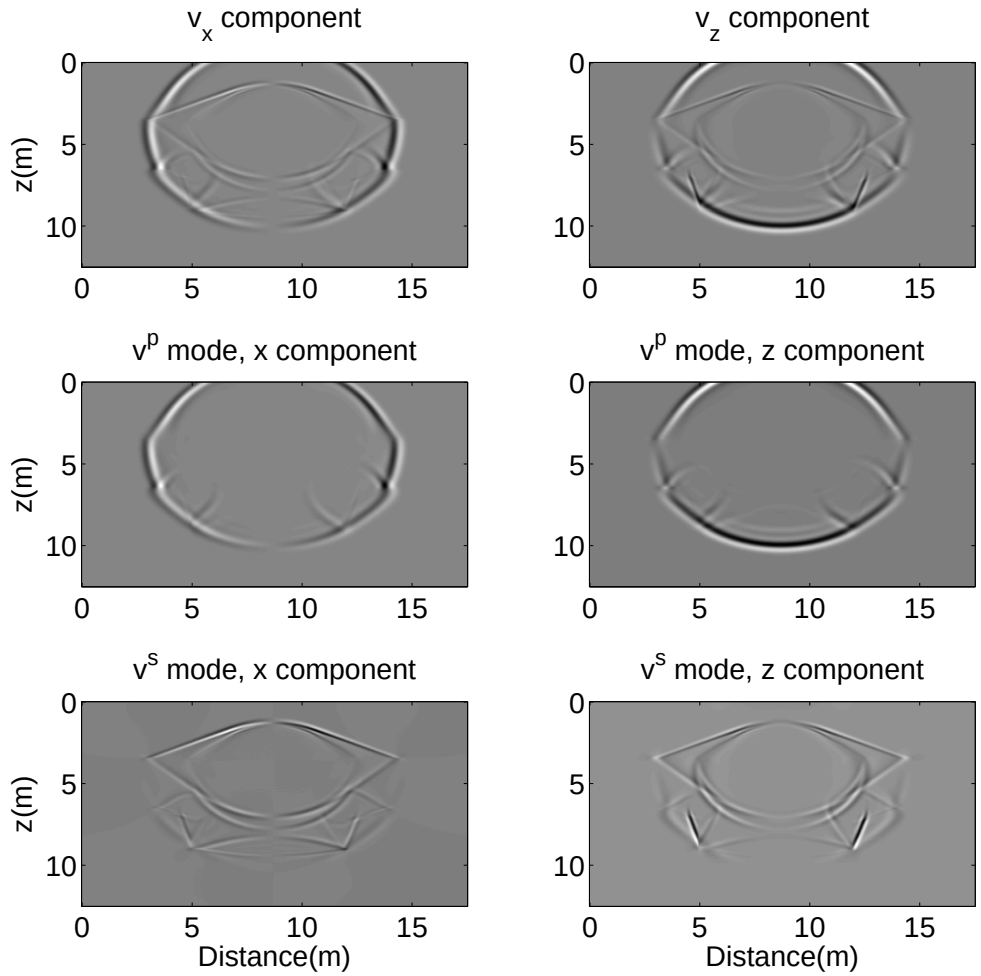

FIG. 5. Original components before decomposition and the corresponding decomposed P- and S-components. First row shows the vertical and horizontal components; second row shows the x- and z-components of the decomposed P-wave and the last row shows the x- and z-components of the decomposed S-wave.

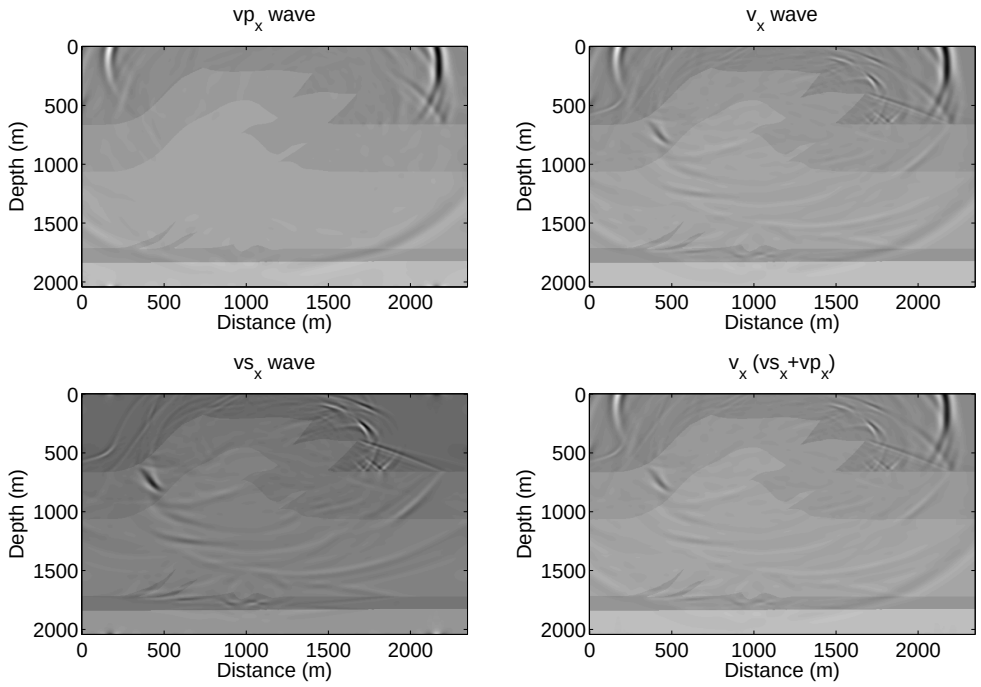

FIG. 6. The decomposed P- and S- wave components and original v_z before decomposition.The combination between the decomposed vp_z and vs_z has the same phase and amplitude with the original v_z mode.

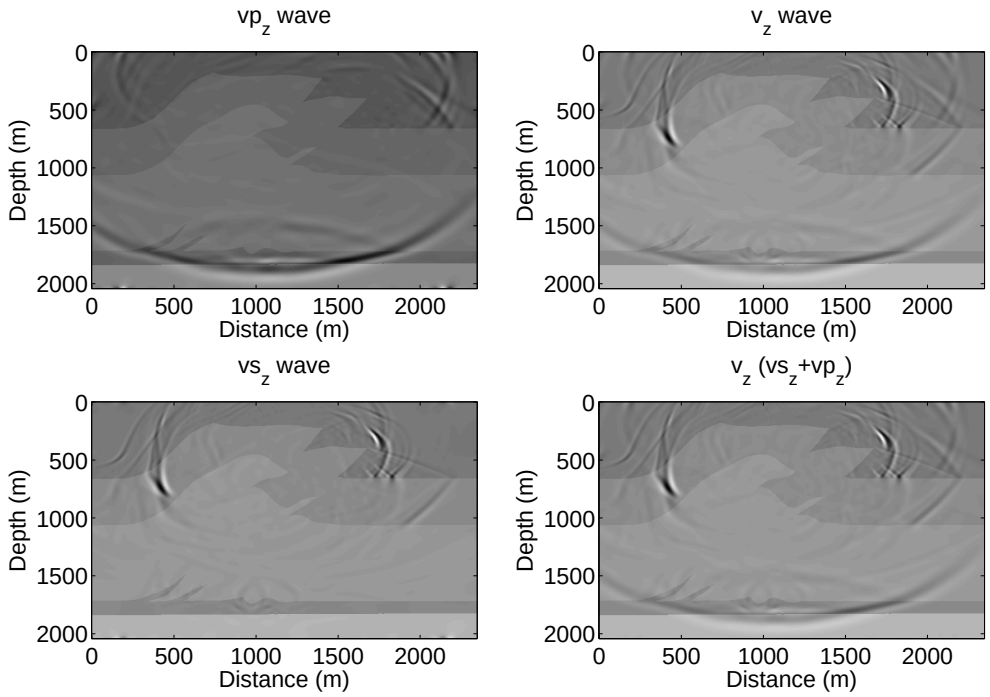

FIG. 7. The decomposed P- and S- wave components and original v_z before decomposition.The combination between the decomposed vp_z and vs_z has the same phase and amplitude with the original v_z mode.

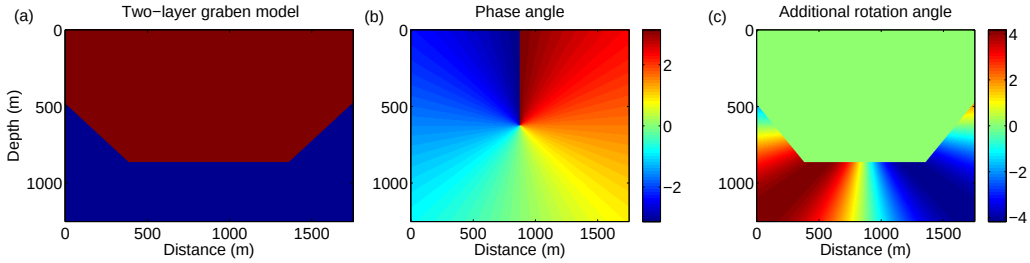

FIG. 8. (a) 2D anisotropic two-layer model, (b) the original phase angle and the additional rotation angle.

Elastic waveform migration for two-layer VTI model

After wave decomposition, each composed component can be used in elastic reverse time migration(ERTM). The images can be obtained from the commonly used imaging condition

$$\int_0^t s(x,\tau)r(x,t-\tau)d\tau. \tag{33}$$

where t is the total recording time, s and r denote the source and receiver P- or S- wavefields.

In this section, a two-layer model is used as an example for decomposed components ERTM, the model is shown in Figure 8 (a), the model size is $2000m \times 1500m$, the first layer is isotropic, with Vp, Vs and density of $4000m/s, 2300m/s, 2000kg/m^3$. The second layer is a VTI formation with $c_11 = 14e9N/m^2, c_13 = 2.1e9N/m^2, c_33 = 17e9N/m^2, c44 = 6.7e9N/m^2$ and density of $2500kg/m^3$. A Ricker wavelet with a dominant frequency of 30 Hz is used as source during forward simulation. The space and time intervals are 5 m and 0.5 ms respectively. Figure 8 (b) and (c) show the original phase angle and the additional rotation angle. We then implement the new waveform decomposition scheme to get separated wave modes, which are further used in ERTM according to equation (33).

Figure 9 shows the PP- PS-, SP- and SS imaging results using ERTM, respectively. The PP- image performs best among the for images, which is barely contaminated by some noise. The PS image suffers some interfering noise, yet the overall imaging result is still acceptable.

CONCLUSIONS

A 3D elastic wave field decomposition scheme for anisotropic media is proposed in this paper, in which the anisotropic polarization vectors' components are determined according to the rotation matrix calculated by the deviation angle. This new scheme solves the uncertainty issue of the polarization vector direction. The decomposition example of a 2D synthetic anisotropic model as well as the anisotropic thrust fault model prove the validity of this new scheme. Finally, the decomposed components are used in ERTM to get the

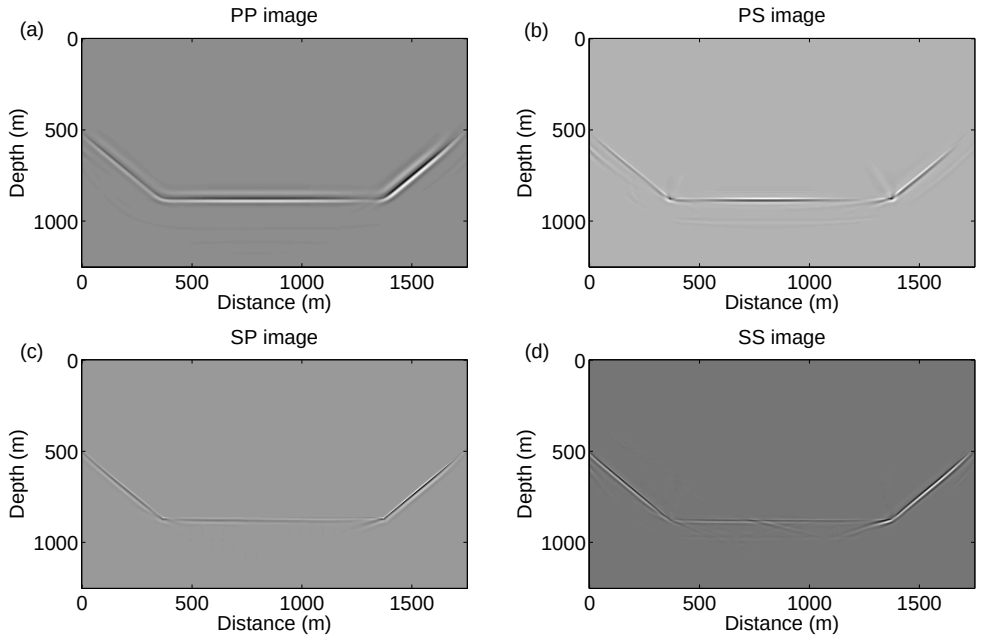

FIG. 9. PP- PS-, SP- and SS imaging results using ERTM.

PP-, PS-, SP- and SS imaging results, the imaging results correlate to the model quite well, which further validates our decomposition method.

For further study, some comparisons for the decomposition methods as well as the imaging results are needed to prove the robustness of the new scheme. Although the 3D elastic wavefield decomposition equations are proposed in this paper, we haven't illustrated any of the 3D decomposition examples, which should be under further study.

ACKNOWLEDGMENTS

This research was supported by the Consortium for Research in Elastic Wave Exploration Seismology (CREWES) and National Science and Engineering Research Council of Canada (NSERC, CRDPJ 379744-08). The first author also thanks to the supporting by SEG and CSEG scholarship.

REFERENCES

Aki, K., and Richards, P. G., 2002, Quantitative seismology, vol. 1:

Chang, W.-F., and McMechan, G. A., 1987, Elastic reverse-time migration: Geophysics, **52**, No. 10, 1365–1375.

Chon, Y.-T., Souza, J., Planchart, C., Lafourcade, P. et al., 2003, Offset vsp imaging with elastic reverse time migration, *in* 2003 SEG Annual Meeting, Society of Exploration Geophysicists.

Dellinger, J., and Etgen, J., 1990, Wave-field separation in two-dimensional anisotropic media: Geophysics, **55**, No. 7, 914–919.

Dellinger, J. A., 1991, Anisotropic seismic wave propagation: Ph.D. thesis, Stanford University.

Dickens, T. A., Winbow, G. A. et al., 2011, Rtm angle gathers using poynting vectors, *in* 2011 SEG Annual Meeting, Society of Exploration Geophysicists.

Lu, R., Traynin, P., Anderson, J. E. et al., 2009, Comparison of elastic and acoustic reverse-time migration on the synthetic elastic marmousi-ii obc dataset, *in* 2009 SEG Annual Meeting, Society of Exploration Geophysicists.

Morse, P. M., Feshbach, H. et al., 1953, Methods of theoretical physics, vol. 1: McGraw-Hill New York.

Rommel, B. E., 1994, Approximate polarization of plane waves in a medium having weak transverse isotropy: Geophysics, **59**, No. 10, 1605–1612.

Slawinski, M. A., 2003, Seismic waves and rays in elastic media, vol. 34: Elsevier.

Sun, R., Chow, J., and Chen, K.-J., 2001, Phase correction in separating p-and s-waves in elastic data: Geophysics, **66**, No. 5, 1515–1518.

Thomsen, L., 1986, Weak elastic anisotropy: Geophysics, **51**, No. 10, 1954–1966.

Tsvankin, I., 2012, Seismic signatures and analysis of reflection data in anisotropic media, 19: SEG Books.

WU, G.-C., LIANG, K., and YIN, X.-Y., 2010, Analysis of phase velocity and polarization features for elastic waves in tti media: Chinese Journal of Geophysics, **53**, No. 4, 658–668.

Yan, J., and Sava, P., 2008, Isotropic angle-domain elastic reverse-time migration: Geophysics, **73**, No. 6, S229–S239.

Zhang, Q., and McMechan, G. A., 2010, 2d and 3d elastic wavefield vector decomposition in the wavenumber domain for vti media: Geophysics, **75**, No. 3, D13–D26.

Zhou, Y., and Wang, H., 2016, Efficient wave mode separation in anisotropic media-part i-separation operators, *in* 78th EAGE Conference and Exhibition 2016.